# INTERFACIAL EVALUATION OF UD-CFRP BY THERMAL AGING VIA ACOUSTIC EMISSION, ELECTRICAL RESISTANCE AND THERMOGRAM METHOD

P.S. Shin[1], D. J. Kwon[1], J. H. Kim[1],
K. L. DeVries[2], J.M. Park[1,2*]

[1] Department of Materials Engineering and Convergence Technology,
Gyeongsang National University, Jinju, Korea
[2] Department of Mechanical Engineering, The University of Utah, Salt Lake City, U. S. A.
* Corresponding author (jmpark@gnu.ac.kr)

**Keywords**: CFRP, Acoustic Emission, Electrical Resistance, Thermogram, ILSS

## ABSTRACT

Interfacial and mechanical properties of thermal aged carbon fiber reinforced epoxy composites (CFRP) were evaluated using acoustic emission (AE), electrical resistance (ER) and thermogram measurements. Unidirectional (UD)-composites were aged at different temperatures to produce different interfacial conditions. AE and ER of UD composites were measured along 0, 30, 60 and 90°. Changes in wavespeed, with thermal aging, were calculated using wave travel time from AE source to AE sensor and the changes in ER were measured. For thermogram evaluation, the composites were laid upon on a hotplate and the increase in the surface temperature was measured. Static contact angle were measured after different thermal aging and elapsed times to evaluate wettability. Interlaminar shear strength (ILSS) and tensile strength tests were also performed to explore the effects of thermal aging on mechanical properties. While thermal aging was found to affect all these properties, the changes were particularly evident at 400 °C.

## 1 INTRODUCTION

Due to some of their unique and superior properties, FRPs are being increasing used in many applications ranging from rehabilitation to construction [1]. Composites are currently being developed for applications in severe environments including cryogenic and high temperature, corrosive environments and exposure to ultraviolet radiation [2, 3] and to assess its location and severity. The extent of damage, caused by exposure to such conditions, is determined using nondestructive evaluation (NDE) procedures, including ultrasonic, radiography, thermography, acoustic emission (AE), modal analysis (such as instrumented tap testing) and eddy-current testing [4, 5]. Recently, in the area of structural health monitoring, polymer conductive composites have received considerable attention due to some of their distinct advantages. [6].

Contact angle measurements are widely used for investigating surface characteristics of materials. The wettability of solid surfaces is an important aspect surface science for a variety of practical applications. The Young-Dupre equation, in terms of the contact angle of a drop of selected liquids on a surface is commonly used to evaluate [7, 8].

Acoustic emission (AE) is important nondestructive evaluation (NDE) tool for the investigation of the mechanisms of micro-failure in structural composite materials. It has been used as a reliable tool for the characterization of structural integrity and to help identify damage mechanisms in complex composite structures under various loading conditions [9, 10]. In these approaches, mechanical and AE information are separately applied to assess behavior of components undergoing mechanical loading [11].

The basic principles underlying the electrical resistance (ER) method of electrical conductive concrete composites are rather straight forward. This method is based on the electrical resistance change (ERC) associated with structural and dimensional changes accompanying the application of stress. Prior research has shown that there in a concomitant increase in ERC with increasing stress conductive composites [12, 13].

This method consists of measurements of the changes of resistance with stress in CFRP specimens and has been shown to provide information on the basic failure mechanisms. The method has been found to have several advantages: the possibility of continuous monitoring of CFRP under loading, the ability to simultaneously detect defects throughout the volume of the specimen, and the possibility of locating and investigating failure mechanisms in the composite structure in real time [14].

Various NDE methods are applied to monitor the static and dynamic failure conditions inside composite materials. Methods based on the acoustic techniques and thermal methods are used to detect defects in the composite structure [15]. The thermogram is solely based on the heat distribution in the system. Thermogram based temperature measurement technique offers many advantages such as prompt response times and ample temperature ranges [16].

In this study, the UD-CFRPs were aged at 200, 300, 400 $^{o}$C with a goal of producing different interfacial conditions to make the different condition of interface. AE and ER sensors were installed along angles of 0, 30, 60 and 90 $^{o}$.The time of travel of waves between the AE source and AE sensor was used to calculate change in wavespeed while ER sensors were used to determine the changes in ER, with aging. For the thermogram evaluation, CFRP specimens were laid on a hotplate and the increase in surface temperature was measured as the hot plate was heated. Changes in static contact angle were also measured, for the different CFRPs, and related to the thermal aging. To investigate the effects of aging on mechanical properties, interlaminar shear (ILSS) and tensile stress tests were conducted. The wavespeed and ER were correlated with the different thermal aging temperatures for the CFRP.

## 2 EXPERIMENTAL

### 2.1 MATERIALS AND SPECIMENS

Carbon fiber (T700SC, Toray Co. LTD., Japan) was used for the composite prepreg (CF preperg, Hankuk Co., Ltd., Korea). Bisphenol A type epoxy was used as resin for the UD composites. The CFRP composites were cut to 100 mm x 100 mm square specimens which were cured a hotpress. These UD-CFRP specimens were supplied by the Hankuk Co., Ltd.

### 2.2 METHODOLOGIES

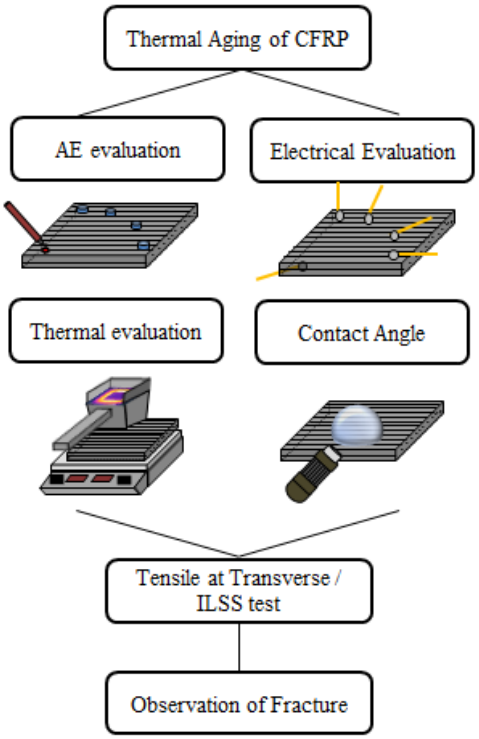


Figure 1: Schematic of interfacial measurement using AE and electrical resistance

AE and ER measurements were used to evaluate changes in the CFRP specimens resulting from thermal aging. Figure 1 shows a schematic arrangement for the interfacial measurements using the AE and ER methods. As a first step, thermal aging of the CFRP was conducted as 200, 300 and 400 $^{o}$C. The aged CFRP specimens were then evaluated by the NDE methods previously described. The sensors were installed along the specified 0, 30, 60 and 90 $^{o}$ directions. The distance between the wave source and sensor for the AE evaluation was 100 mm.

An oscilloscope (LT584, Lecroy, U.S.A.) was used to measure the wavespeed. The AE sensors were fixed on both two sides of the specimen with as pacing of 100 mm. The wavespeed was calculated by the time for the wave to travel between the source and the sensor by the equation:

$$\mathrm{v} = \frac{l}{s} \tag{1}$$

where, v is the wavespeed, l is distance between wave source and sensor and s is the wave travel time [17].

The electrical resistance of the CFRP composite specimens was determined by the four-probe method using a multimeter (HP34401A) [18]. The specimen's electrical resistivity was determined by means of electrical contact points, using embedded copper wire without silver paste, located at regularly spaced intervals, along the specimen. The resistivity is the resistance per unit volume of the bulk material, and its determination provides a measure of the state of dispersion of the CNT filler in composites. The equation used for calculation of this electrical resistivity is:

$$\rho_v = \left(\frac{A_v}{L_{ec}}\right) \times R_v \tag{2}$$

where $\rho_v$ is the resistivity, $R_v$ is the measured electrical resistance, $A_v$ is the cross-sectional area, and $L_{ec}$ is the spacing between the electrical contact points [19].

Wettability was determined from static contact angles using uniform micro-droplets of double purified water. Uniform micro-droplets were each positioned on the surfaces of specimen of the different CFRP. These measured angles are related to the surface tensions by Young's equation:

$$\gamma_S - \gamma_{SL} = \gamma_L cos\theta \tag{3}$$

where, where θ is the measured contact angle, $\gamma_L$ is the surface tension of the liquid, $\gamma_{SL}$ is the interfacial energy between the solid and the liquid, and $\gamma_S$ is the surface energy of the solid substrate [20, 21].

To measure the mechanical properties of specimens, the short beam test (ASTM D-2344) and tensile tests (in the transverse direction) were performed on specimens with the different aging histories. A UTM (H1KS, Lloyd, U.S.A.) at a cross-head speed of 1 mm/minute was used in these tests. The equation used to determine the ILSS from the test results is:

$$\tau = \frac{3P_{max}}{4Bd} \tag{4}$$

where $P_{max}$ is the load at the center of the short beam specimen, B is the thickness and d is the width of test specimen [22, 23].

## 3 RESULTS AND DISCUSSION

### 3.1 AE and ER evaluation of CFRP aging

Figure 2 shows the AE wavespeeds in the specified directions for the CFRP after the indicated different thermal aging treatments. Initially, the wavespeed in the longitudinal direction was higher than it was in the transverse direction. The wavespeed in the longitudinal direction decreased more rapidly with thermal aging than the wavespeed in the transverse direction. This was especially true for the 400 $^{o}$C aging where the decrease was 597 m/s. It is thought that these affects might be related to microcracking between fiber and matrix, during aging, tending to retard the wave motion.

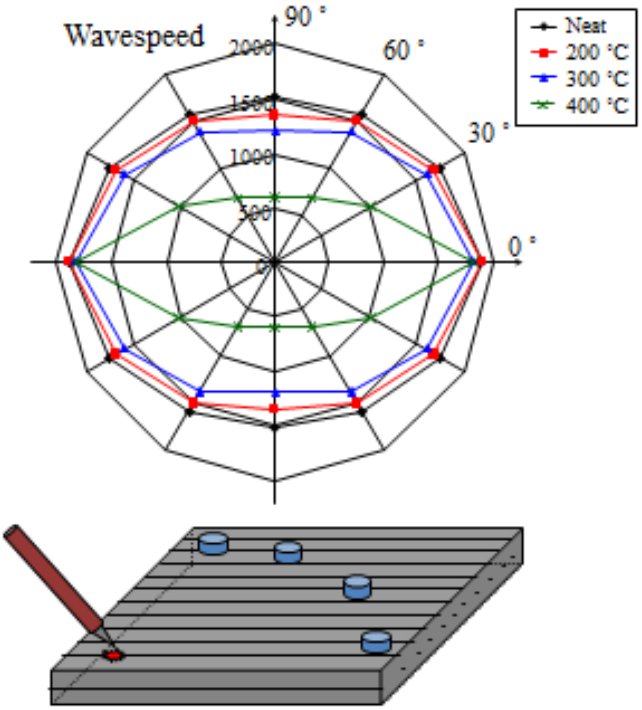


Figure 2: Wavespeeds of each directions of CFRP after aging treatment

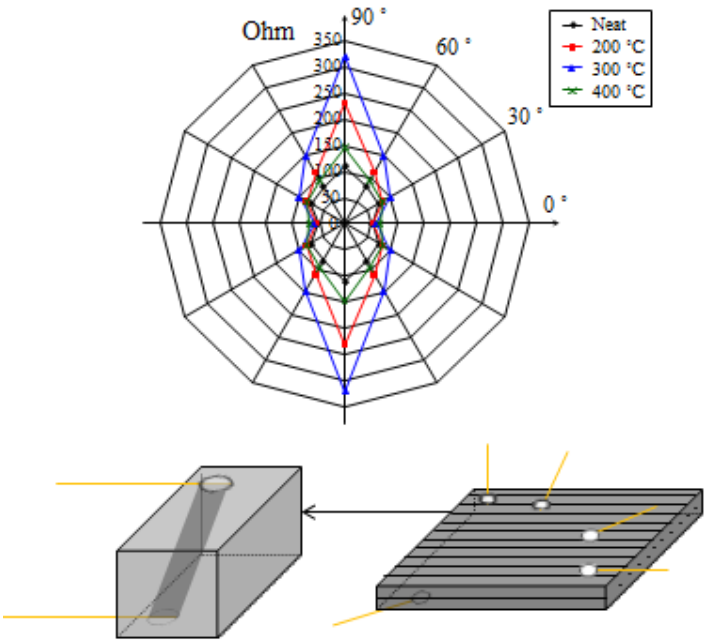


Figure 3: Electrical Resistance of each directions of CFRP after aging treatment

Figure 3 shows results of the ER tests for each of the specified directions on the CFRP specimens, after the indicated thermal aging treatments. Initially, the ER in the longitudinal direction was lower than that for the transverse direction. With thermal aging the ER in the longitudinal direction increase more rapidly than it did in the transverse direction. It is hypotheses that these affects are related to microcracking between fiber and matrix, during thermal aging, which would tend to interrupt electrical flow in the material thereby increasing the ER.

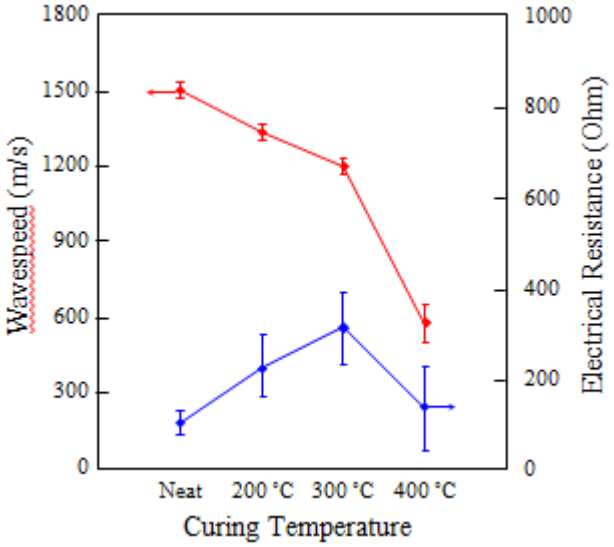


Figure 4: Electrical Resistance and wavespeed of transverse direction of CFRP after aging treatment

Figure 4 shows the ER and wavespeed in the transverse direction for CFRP after the different aging treatments. The wavespeed decreased while the ER increased for the thermal treatment up to 300 $^{o}$C. After the 400$^{o}$C treatment, both the wave and the ER exhibited significant decreases. It appears that for aging at temperatures up to 300 $^{o}$C there were significant but rather gradual changes in wave velocity and ER but 400 $^{o}$C aging resulted in much more dramatic changes and in the case of ER evens a reversal in the direction of the change.

### 3.2 Thermal and surface properties

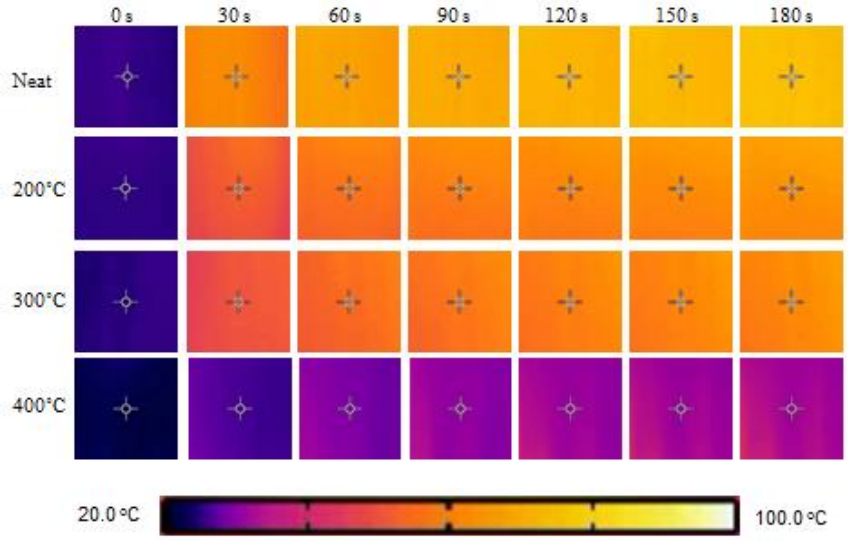


Figure 5: Thermogram of heat transfer of CFRP after aging treatment: (a) neat; (b) 200˚C; (c) 300 ˚C and (d) 400 ˚C

Figure 5 shows a thermogram for heat transfer in the CFRP after the different thermal aging treatments. It is seen that the color of thermogram changed with changes in thermal aging. For the neat CFRP, the color changed from bright purple to nearly yellow, the 200 and 300 $^{o}$C treated CFRP the change was from purple to orange, whereas for the 400 $^{o}$C treated CFRP the color change was from blackish-violet to bright purple. These color changes might be viewed as indicators of changes in the degree or extent of heat transfer in the CFRP specimens.

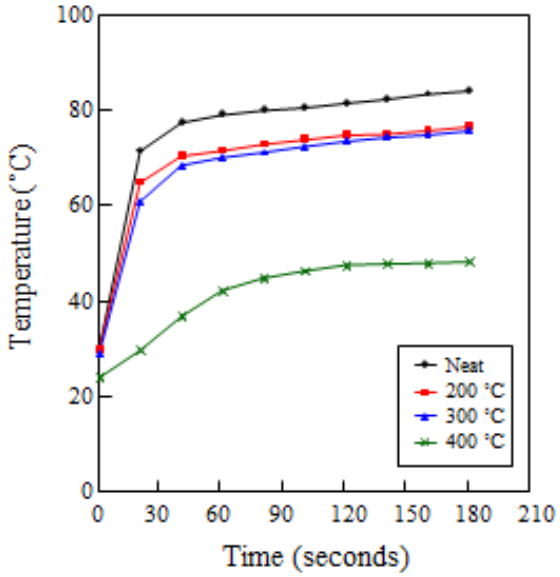


Figure 6: Change of heat transfer of CFRP after aging treatment

Figure 6 shows the change in heat transfer in CFRP after different thermal aging treatments. The temperature increased rapidly during the first 20 seconds and then much more gradually. The degree of thermal transfer was largest for the neat CFRP dramatically less for CFRP treated at 400 $^{o}$C. For example, at 180 seconds the temperature of the neat material had increased to 84.4 $^{o}$C, while at the same time the temperature of the material aged at 400 $^{o}$C had only increased to 48.4 $^{o}$C.

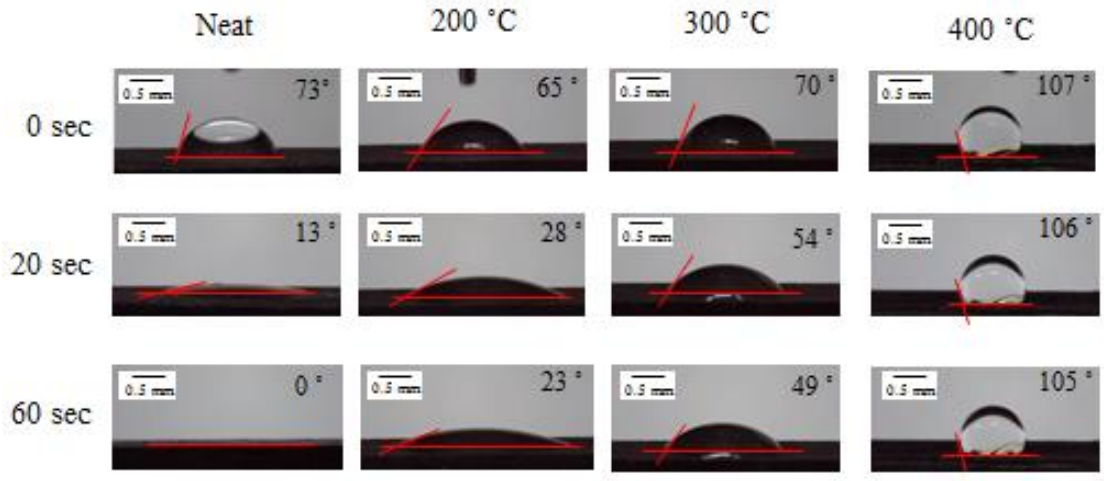


Figure 7: Change of static contact angle on different thermal aging CFRP

The photographs in figure 7 clearly illustrate the differences in the static contact angles for droplets of water on CFRP with the different thermal aging treatments. For neat CFRP, the initial contact angle was 73 $^{o}$ and the contact angle rapidly decreased with time such that. After 60 seconds contact angle was essentially 0$^{o}$ as the water was almost completely absorbed into the CFRP. Somewhat similar behavior, but at a reduced rate, was observed for the CFRP that had been aged at 200 $^{o}$C and 300 $^{o}$C.

However, for material aged at 400 $^{o}$C the initial contact angle was 107 $^{o}$ and it experienced very little change during the 60 second observation period. It could be due to exposed hydrophobic carbon fiber by thermal treatment, which resulted in the elimination of epoxy resin on the surface. Figure 8 shows the change in static contact angle as a function of time for GFRP with the different aging treatments. Figures 7 and 8 together clearly demonstrate the dramatic difference thermal aging has on wetting behavior.

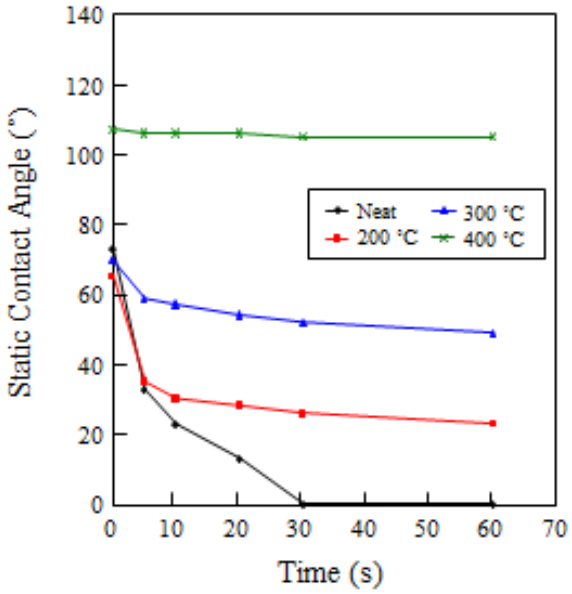


Figure 8: Static contact angle of CFRP as different aging temperature

### 3.3 Mechanical and interfacial properties and modeling of CFRP after thermal aging

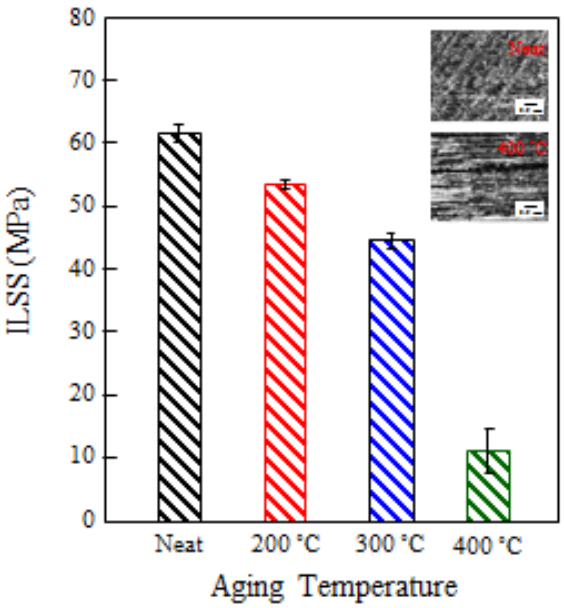


Figure 9: ILSS test of CFRP after aging treatment

Figure 9 shows the results of ILSS short beam testing on GFRP specimens with the different thermal aging treatments. The ILSS decreased from approximately 60 MPa for the neat material to roughly 10 MPa for material aged at 400 $^{o}$C. As with the other properties, discussed previously, the ILSS decreased significant but rather gradually up to an aging temperature of 300 $^{o}$C, but experienced a very dramatic decrease for GFRP aged at 400 $^{o}$C. This dramatic decrease in ILSS was accompanied by a significant increase in micro cracking.

Figure 10 shows the results of tensile testing in the transverse direction of CFRP after the different thermal aging treatments. The tensile strength for neat CFRP was approximately 65 MPa but only 5 MPa for the CFRP aged 400 $^{o}$C. Figure 10 also shows a couple of FE-SEM photographs of tensile a neat specimens and a specimen aged at 400 $^{o}$C. These clearly illustrate differences in which the resin and carbon fibers that are initially connected at their interface becomes more disconnected during the 400 $^{o}$C aging, as some of the epoxy evaporated or was otherwise degraded and removed.

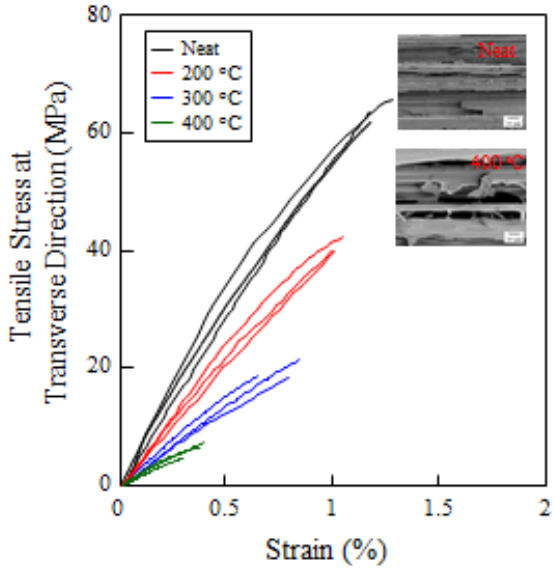


Figure 10: Tensile test of transverse direction of CFRP after aging treatment

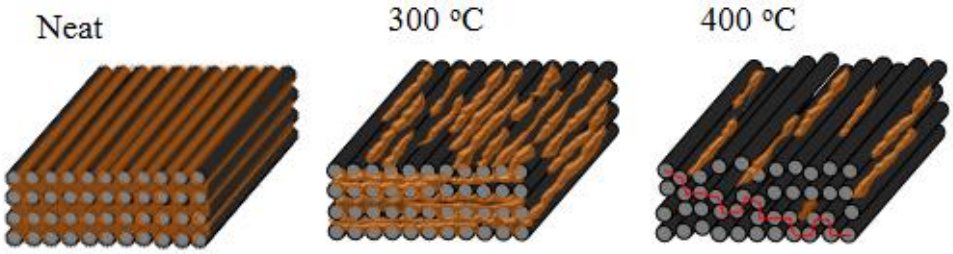


Figure 11: Schematic diagram of CFRP after thermal aging:

Figure 11 shows schematic modeling of CFRP after different thermal aging treatments. In the neat condition, the carbon fibers are effectively covered with and bonded to the matrix. During thermal treatment the composites damaged in that weakly bonded and relatively thermally weak polymer matrix is removed. This affects the acoustic properties resulting in a decrease in wavespeed, as well as a decrease in electrical conductivity. These models also provide an indication on why aging should affect ILSS and tensile strength (particularly in the transverse direction).

## 4 CONCLUSIONS

UD-CFRPs were aged at 200, 300, 400 $^{o}$C resulting in different interfacial conditions and properties. AE, ER and thermogram measurements were used to investigate aging produced changes in the CFRP properties. For the AE and ER studies sensors were installed along angles of 0, 30, 60 and 90 $^{o}$. AE and ER measurements revealed that the wavespeed decreased while the ER increased for aging treatment up to 300 $^{o}$C followed by a very large decrease in wavespeed and a large decrease in conductivity for specimens aged at 400 $^{o}$C. The rate of heat transfer was best in neat CFRP and it experienced a rather gradual decrease up to an aging temperature of 300 $^{o}$C followed by a very significant drop for CFRP aged at treated at 400 $^{o}$C. Water droplet contact angles and there changes with time were found to be dependent on thermal aging treatment. For the neat CFRP the initial contact angle was just over 70 $^{o}$ and rapidly decreased to essentially 0$^{o}$ after 60 seconds as the water appeared to be absorbed into the composite. Aging of the CFRP dramatically changed its wetting behavior. The rate of spreading gradually decreased with aging temperature up to 300 $^{o}$C after which a large change occurred and there was almost no spreading evident during the 60 second observation period for material aged ILSS and tensile test results exhibited trends similar to those just described. Both the IISS and tensile strength decreased significantly but relatively gradually with aging up to 300 $^{o}$C but dropped precipitously for the material aged at 400 $^{o}$C. Measurement related to heat transfer and

FE-SEM observations provided further evidence for thermal aging induced structural damage of the composite. Experiments in which CFRP specimens, with the different aging histories, were placed on a hot plate and their surface temperature measure as a function of time, clearly demonstrated that thermal aging, particularly at 400 $^{o}$C, reduced the composite's heat transfer capability. FE-SEM photographs showed that resin-fiber bonding and resin integrity was greatly diminished in the CFRP aged at 400 $^{o}$C.

## ACKNOWLEDGEMENTS

This work was supported by the Korea Institute of Energy Technology Evaluation and Planning (KETEP) and the Ministry of Trade, Industry & Energy (MOTIE) of the Republic of Korea (No. 20163030024550).

## REFERENCES

1. Shin PS, Wang ZJ, Kwon DJ, Choi JY, Sung Il, Jin DS, et al. Optimum mixing ratio of epoxy for glass fiber reinforced composites with high thermal stability. Compos Part B Eng 2015;79:132–7.
2. Vijay P V., Soti PR, GangaRao HVS, Lampo RG, Clarkson JD. Design and evaluation of an integrated FRP composite wicket gate. Compos Struct 2016;145:149–61.
3. Park JM, Shin PS, Wang ZJ, Kwon DJ, Choi JY, Lee S Il, et al. The change in mechanical and interfacial properties of GF and CF reinforced epoxy composites after aging in NaCl solution. Compos Sci Technol 2016;122:59–66.
4. Carra G, Carvelli V. Ageing of pultruded glass fibre reinforced polymer composites exposed to combined environmental agents. Compos Struct 2014;108:1019–26.
5. Ambu R, Aymerich F, Ginesu F, Priolo P. Assessment of NDT interferometric techniques for impact damage detection in composite laminates. Compos Sci Technol 2006;66:199–205.
6. Zhang D, Ye L, Wang D, Tang Y, Mustapha S, Chen Y. Assessment of transverse impact damage in GF/EP laminates of conductive nanoparticles using electrical resistivity tomography. Compos Part A Appl Sci Manuf 2012;43:1587–98.
7. Wang ZJ, Kwon DJ, Gu GY, Devries KL, Park JM. Surface control and cryogenic durability of transparent CNT coatings on dip-coated glass substrates. J Colloid Interface Sci 2012;386:415–20.
8. Hsieh CT, Li CT, Shih HC, Lin TS, Wu CF. Influence of fluorine/carbon atomic ratio on superhydrophobic behavior of carbon nanofiber arrays. , J Vac SciTechnol 2006;24:113
9. Todoroki A, Tanaka Y, Shimamura Y. Delamination monitoring of graphite/epoxy laminated composite plate of electric resistance change method. Compos Sci Technol 2002;62:1151–60.
10. Liu L, Li L, Gao Y, Tang L, Zhang Z. Single carbon fiber fracture embedded in an epoxy matrix modified by nanoparticles. Compos Sci Technol 2013;77:101–9.
11. Todoroki A, Tanaka Y. Delamination identification of cross-ply graphite / epoxy composite beams using electric resistance change method. Compos Sci Technol 2002;62:629–39.
12. Selman E, Ghiami A, Alver N. Study of fracture evolution in FRP-strengthened reinforced concrete beam under cyclic load by acoustic emission technique: An integrated mechanical-acoustic energy approach. Constr Build Mater 2015;95:832–41.
13. Shabana YM, Noda N. Numerical evaluation of the thermomechanical effective properties of a functionally graded material using the homogenization method. Int J Solids Struct 2008;45:3494–506.
14. Kim H, Cho JW, Song I, Min KB. Anisotropy of elastic moduli, P-wave velocities, and thermal conductivities of Asan Gneiss, Boryeong Shale, and Yeoncheon Schist in Korea. Eng Geol 2012;147–148:68–77.
15. Gadomski J, Pyrzanowski P. Experimental investigation of fatigue destruction of CFRP using the electrical resistance change method. Meas J Int Meas Confed 2016;87:236–45.

16. Zainui AJ, Ashwani KD. Design of early fault detection technique for electrical assets using infrared thermograms. International journal of electrical power & energy systems 2014;63:753-9.
17. Selmy AI, Elsesi AR, Azab NA, Abd El-Baky MA. Interlaminar shear behavior of unidirectional glass fiber (U)/random glass fiber (R)/epoxy hybrid and non-hybrid composite laminates. Compos Part B Eng 2012;43:1714–9.
18. Liu YL. Flame-retardant epoxy resins from novel phosphorus-containing novolac. Polymer (Guildf) 2001;42:3445–54.
19. Rahman MM, Zainuddin S, Hosur M V., Robertson CJ, Kumar A, Trovillion J, et al. Effect of NH 2-MWCNTs on crosslink density of epoxy matrix and ILSS properties of e-glass/epoxy composites. Compos Struct 2013;95:213–21.
20. Park JM, Gu GY, Wang ZJ, Kwon DJ, DeVres KL, Interfacial durability and acoustical properties of transparent graphene nano platelets/poly (vinylidene fluoride) composite actuators. Thin Solid Films 2013;31:350-355.
21. Park JM, Gu GY, Wang ZY, Kwon DJ, DeVres KL, Interfacial durability and electrical properties of CNT or ITO/PVDF nanocomposites for self-sensor and micro actuator applications. Appl Surf Sci 2013;287:75-83.
22. Wang ZJ, Kwon DJ, Gu GY, Kim HS, Kim DS, Lee CS, et al. Mechanical and interfacial evaluation of CNT/polypropylene composites and monitoring of damage using electrical resistance measurements. Compos Sci Technol 2013;81:69–75.
23. Borri A, Corradi M, Grazini A. A method for flexural reinforcement of old wood beams with CFRP materials. Compos Part B Eng 2005;36:143–53.